Frequency-domain analysis for nonlinear systems with time-domain model parameter uncertainty

William R. Jacobs, Tony Dodd, and Sean R. Anderson

Abstract—Frequency-domain analysis of dynamic systems is important across many areas of engineering. However, whilst there are many analysis methods for linear systems, the problem is much less widely studied for nonlinear systems. Frequency-domain analysis of nonlinear systems using frequency response functions (FRFs) is particularly important to reveal resonances, super/sub-harmonics and energy transfer across frequencies. In this paper the novel contribution is a time-domain model-based approach to describing the uncertainty of nonlinear systems in the frequency-domain. The method takes a nonlinear input-output model that has normally distributed parameters, and propagates that uncertainty into the frequency-domain using analytic expressions based on FRFs. We demonstrate the approach on both synthetic examples of nonlinear systems and a real-world nonlinear system identified from experimental data. We benchmark the proposed approach against a brute-force technique based on Monte Carlo sampling and show that there is good agreement between the methods.

Index Terms—nonlinear systems, frequency domain, uncertainty propagation

I. INTRODUCTION

The frequency response is an important method of analysing system dynamics and designing control systems. There are standard methods for analysing the frequency response of both linear and nonlinear systems using time-domain models obtained from system identification techniques [1], [2]. For nonlinear systems, frequency-domain analysis methods from time-domain models include the generalised frequency response functions (GFRFs) [3] and the nonlinear output frequency response functions (NOFRFs) [4], which both aid in analysing phenomena such as sub- and super-harmonics as well as resonances and energy transfer between frequencies [5], [6].

A further key aspect for analysis and design in the frequency-domain is the characterisation of uncertainty. For linear systems, it is straight-forward to identify a time-domain model with uncertainty estimates for the parameters, from this obtain a transfer function description, and then use model-based methods for analysing uncertainty in the frequency-domain [7]–[9]. However, similar methods have not yet been developed for analysing uncertainty in the frequency-domain from identified time-domain models of nonlinear systems, which is a key gap in the literature. This is except for the brute-force approach of using numerical sampling to map uncertainty from a time-domain nonlinear model to a corresponding frequency response function (FRF), which is

W. R. Jacobs, T. Dodd, and S. R. Anderson are with the Department of Automatic Control and Systems Engineering, University of Sheffield, Sheffield, S1 3JD UK, e-mail: w.jacobs@sheffield.ac.uk

computationally expensive [10]. The aim of this paper is to address the problem of analytically mapping uncertainty from a time-domain nonlinear model to the GFRFs and NOFRFs in a computationally efficient manner, significantly extending the usefulness of models obtained from nonlinear system identification.

The approach taken here for solving the problem of mapping uncertainty from the time-domain nonlinear model to the FRFs is based on uncertainty propagation. The propagation of uncertainty for real-valued quantities is well understood, and is routinely used for calculating experimental measurement uncertainty across various scientific domains [11]. However, FRFs are complex-valued, *i.e.* they consist of a real and imaginary part, whilst parameter uncertainty in the time-domain model is real-valued, and so uncertainty propagation is more complicated in this scenario.

For complex-valued data, the propagation of uncertainty has not been widely studied but there are two main approaches that can be taken.

In one approach, the complex statistics method estimates the uncertainty in a complex variable as a symmetrical normal distribution in the real-imaginary space, such that its variance can be quantified by a single number [12]. The limitation of this method is that uncertainty is constrained to be the same in both the real and imaginary dimensions due to the use of a symmetrical normal distribution.

In the alternative approach, the multivariate uncertainty method assigns a bi-variate normal distribution to the complex variable such that a covariance matrix describes the correlation of the real and imaginary parts [13], [14]. This method can hence offer a more flexible and accurate description because it can represent the uncertainty as an ellipse rather than a circle (compared to the complex statistics method). Multivariate uncertainty propagation has been applied to quantifying the measurement uncertainty in experimentally gathered data [15], [16] and to finite-element models [17].

In this paper, we develop a novel method for the model-based frequency-domain uncertainty analysis of nonlinear systems based on the second approach described above: multivariate uncertainty propagation, under the assumption that model parameters are normally distributed, and that uncertainties satisfy the local linear approximation. The method is applicable to both identified nonlinear models and also physically derived models and has the important novel feature that it can analytically generate uncertainty bounds for both the GFRFs and the NOFRFs.

The paper is structured as follows. In section II we review FRFs for nonlinear systems and the treatment of complex

numbers as random variables. In section III we develop uncertainty propagation for nonlinear models. In section IV we demonstrate the analysis method on a simulated example and a nonlinear model identified from experimental data. Finally, the paper is summarised in section V.

II. PROBLEM FORMULATION

In this section we motivate the problem of propagating uncertainty into the FRF from the time-domain model parameters and background is given on how uncertainty can be approximately propagated through some nonlinear function into a complex output variable.

A. Nonlinear time-domain model with uncertain parameters

A single-input single-output nonlinear dynamic system can be described by a nonlinear function, $f(.)$, of input-output signals, [2], [18],

$$y_k = f\left(y_{k-1}, ..., y_{k-n_y}, u_{k-1}, ..., u_{k-n_u}\right) \quad (1)$$

where $u_k \in \mathbb{R}$, for $k = 1, \ldots, n_u$ are lagged system inputs, and $y_k \in \mathbb{R}$, for $k = 1, \ldots, n_y$ are lagged system outputs with respect to sample time k. The non-linear function $f(\cdot)$ can then be decomposed into a sum of weighted basis functions, where the basis functions can be from a wide class, e.g. polynomial, radial, B-spline, [19],

$$f(\mathbf{x}_k) = \sum_{m=1}^{M} \theta_m \phi_m(\mathbf{x}_k) \quad (2)$$

where $\theta_m \in \mathbb{R}$ is the mth model parameter, $\phi_m(\mathbf{x}_k)$ is the mth basis function, $\mathbf{x}_k = \left(y_{k-1}, ..., y_{k-n_y}, u_{k-1}, ..., u_{k-n_u}\right)$ and M is the total number of model terms. The model can be written more compactly as

$$f(\mathbf{x}_k) = \phi_k \boldsymbol{\theta} \quad (3)$$

where $\boldsymbol{\theta} = (\theta_1, \ldots, \theta_M)^T$, $\phi_k = (\phi_1(\mathbf{x}_k), \ldots, \phi_M(\mathbf{x}_k))$.

We assume here that the parameters can be described by a normal distribution,

$$\boldsymbol{\theta} \sim N(\bar{\boldsymbol{\theta}}, \Sigma_\theta) \quad (4)$$

where in practice an estimate of the parameter mean and covariance can be obtained e.g. via least-squares [18] or Bayesian estimation [20].[1]

The key problem addressed here is the propagation of the time-domain model parameter uncertainty, characterised by the parameter covariance, Σ_θ, into the frequency-domain. This propagation gives uncertainty bounds on the magnitude and phase of frequency response functions used to analyse nonlinear dynamics .

[1]To reduce parameter bias resulting from measurement noise in y_k, the model could be extended, e.g. to include a noise model with estimation by pseudo-linear regression [2], or to a state-space framework that explicitly includes measurement noise, with estimation by expectation-maximisation, the EM-algorithm [21].

B. Generalised frequency response functions: GFRFs

The dynamics of nonlinear systems can be analysed in the frequency-domain from time-domain models of the form given in (3) using generalised frequency response functions (GFRFs) [3].

To define the GFRFs, note that the output spectrum, $Y(j\omega)$, of a wide class of nonlinear system can be described by [2],

$$Y(j\omega) = \sum_{n=1}^{N} Y_n(j\omega) \quad (5)$$

where

$$Y_n(j\omega) = \frac{n^{-1/2}}{(2\pi)^{n-1}} \int_\omega H_n(j\omega_1, \ldots, j\omega_n) \prod_{i=1}^{n} U(j\omega_i) \mathrm{d}\sigma_{n\omega}, \quad (6)$$

where $\int_\omega F_n(j\omega_1, \ldots, j\omega_n) \mathrm{d}\sigma_{n\omega}$ denotes the integral of $F_n(j\omega_1, \ldots, j\omega_n)$ over the n-dimensional hyperplane $\omega = \omega_1 + \ldots + \omega_n$, and the GFRF is defined as

$$H_n(j\omega_1, \ldots, j\omega_n) = \int_{-\infty}^{\infty} \cdots \int_{-\infty}^{\infty} h_n(\tau_1, \ldots, \tau_n) e^{-j(\omega_1\tau_1 + \ldots + \omega_n\tau_n)} \mathrm{d}\tau_1 \ldots \mathrm{d}\tau_n \quad (7)$$

where $h_n(k_1, \ldots, k_n)$ is the nth-order Volterra kernel, or equivalently the nth impulse response function of the system.

The GFRFs can be calculated using the probing method, where sinusoidal excitation is applied to a model of the nonlinear system [3], [22]. The probing method gives an explicit link between the time-domain model in (3) and frequency-domain analysis of the nonlinear system.

Whilst GFRF-based analysis of nonlinear systems is useful, it is also limited in the sense that it is not possible to visualise GFRFs above second order. Therefore, it is not possible to realise the same intuitive interpretation of nonlinear dynamics with GFRFs as it is with linear systems using Bode plots.

C. Nonlinear output frequency response functions: NOFRFs

The nonlinear output frequency response functions (NOFRFs) characterise the nonlinear system dynamics using input-specific one-dimensional frequency response functions [4]. Both of these aspects provide key advantages over GFRFs: 1. GFRFs are not input-specific, which is a limitation because nonlinear system responses are input-dependent; 2. GFRFs are multi-dimensional, which inhibits analysis for nonlinear orders greater than two. As shown below, the NOFRFs allow the nth-order output spectra in (5) to be described in a manner similar to linear systems, which highly simplifies analysis and design for nonlinear systems in the frequency-domain.

To define the NOFRFs, we first extend the definition of the output spectrum of the nonlinear system in (5), so that

$$Y(j\omega) = \sum_{n=1}^{N} Y_n(j\omega) = \sum_{n=1}^{N} G_n(j\omega) U_n(j\omega) \quad (8)$$

where $U_n(j\omega)$ is an input signal designed by the user that can include specific frequencies and amplitudes (see Appendix for details) and the NOFRF is

$$G_n(j\omega) = \frac{\int_{-\infty}^{\infty} \cdots \int_{-\infty}^{\infty} H_n(j\omega_1, \ldots, j\omega_n) \prod_{i=1}^{n} U(j\omega_i) \mathrm{d}\omega_1 \ldots \mathrm{d}\omega_n}{\int_{-\infty}^{\infty} \cdots \int_{-\infty}^{\infty} \prod_{i=1}^{n} U(j\omega_i) \mathrm{d}\omega_1 \ldots \mathrm{d}\omega_n}$$
(9)

under the condition that $U_n(j\omega) \neq 0$, where

$$U_n(j\omega) = \frac{n^{-1/2}}{2\pi^{n-1}} \int_{-\infty}^{\infty} \cdots \int_{-\infty}^{\infty} \prod_{i=1}^{n} U(j\omega_i) \mathrm{d}\omega_1 \ldots \mathrm{d}\omega_n \quad (10)$$

The decomposition of the nth-order output spectra, $Y_n(j\omega)$, into the product of the NOFRFs, $G_n(j\omega)$, and n^{th}-order input spectra provides an important advantage over GFRFs in that the nonlinear effects of specific input signals can be analysed (in a one-dimensional form). For instance, analysis of the individual NOFRFs, $G_n(j\omega)$, can reveal resonant modes at different orders of nonlinearity. In addition, reconstruction of the nth output spectra, $Y_n(j\omega)$, using the NOFRFs, permits analysis of inter-kernel mixing effects, showing how energy is transmitted across frequencies.

The NOFRF, $G_n(j\omega)$, is a function of the GFRF, $H_n(j\omega_1, \ldots, j\omega_n)$. So, naively, it would seem that it is necessary to obtain the GFRF before calculating the NOFRF, which is relatively long-winded and computationally expensive. However, a simpler and more efficient algorithm has been developed to calculate NOFRFs numerically, which by-passes the need to explicitly calculate the GFRFs [4]. This algorithm is model-based, in that it uses simulations of the model for various excitation signals to determine the NOFRFs from fast Fourier transforms of the input-output data. The algorithm is described in the Appendix A.

The description above shows how a nonlinear system can be analysed in the frequency-domain using either GFRFs and/or NOFRFs. The key novel problem addressed here is the propagation of uncertainty into the frequency-domain using a time-domain model with uncertain parameters, characterised by a covariance matrix Σ_θ. Simplistically, uncertainty in the GFRF or NOFRF can be propagated by Monte Carlo simulations. However, this is a crude approach, which is relatively computationally expensive, and a more elegant analytic theory can be derived based on uncertainty propagation.

D. Uncertainty in complex valued quantities

When considering the uncertainty associated with a real valued measurement of a system it is very common to assume that the variable is drawn from a normal probability distribution [23]. The assumption of normality allows the distribution to be defined by the statistics of the normal distribution, the mean μ and the variance σ^2. The uncertainty can then be displayed by a percentage confidence interval which defines the interval in which the measurement falls within a percentage probability, see Figure 1A.

When the measurement is drawn from a bivariate normal distribution the statistics are defined by the vector mean μ and covariance given by

$$\Sigma = \begin{bmatrix} \sigma_{1,1} & \sigma_{1,2} \\ \sigma_{2,1} & \sigma_{2,2} \end{bmatrix}$$
(11)

where $\sigma_{1,1}$, $\sigma_{2,2}$ are the variance in the 1st and 2nd variate respectively and $\sigma_{1,2} = \sigma_{2,1}$ is the covariance between the two. The mean and covariance matrix define a probability distribution in the space of two variates that characterise the uncertainty. Analogous to the univariate measurement where the uncertainty can be displayed as a confidence interval, for the bivariate measurement a percentage confidence area is defined by the uncertainty in each variate and the correlation between them [24]. In the space of the two variates the confidence area is elliptical.

A complex valued variable is often represented in two parts, real and imaginary (commonly plotted on an Argand diagram), where

$$x = a + jb = \mathrm{Re}(x) + j\,\mathrm{Im}(x).$$
(12)

Complex variables can hence be though of as bivariate:

$$X = [\mathrm{Re}(x), \mathrm{Im}(x)].$$
(13)

In general the variance in the real and imaginary parts of the measurement will not be independent and can therefore be assumed to be drawn from the bivariate normal distribution

$$X \sim \mathcal{N}\left(X \Big| \begin{bmatrix} \mu_{\mathrm{Re}(x)} \\ \mu_{\mathrm{Im}(x)} \end{bmatrix}, \Sigma_{\mathrm{Re}(x),\mathrm{Im}(x)} \right).$$
(14)

The uncertainty in a complex variable is then displayed as an elliptical confidence area in the real-imaginary space, see Figure 1B. Another alternative representation for complex variables is in gain-phase form, this is common practice when considering systems in the frequency domain [1]. The gain-phase representation of a complex variable can also be considered as bivariate and so can be treated similarly. Care should be taken when using the gain-phase representation however because the uncertainty predictions at near zero gain can be inaccurate in some cases, see [13].

E. Classical uncertainty propagation

Propagation of uncertainty is the calculation of the uncertainty associated with the output of some function by considering the uncertainty in its input variables and how these *propagate* through the equation. A discussion of the classical treatment of uncertainty propagation follows.

Firstly consider a function f which is a linear combination of p variables $x_1, x_2, \ldots, x_p$ with coefficients $c_1, c_2, \ldots, c_p$, such that

$$y = f(x_1, x_2, \ldots, x_p) = \sum_{i=1}^{p} c_i x_i = \mathbf{cx}$$
(15)

where the uncertainty associated with the input variables is described by the covariance matrix

$$\Sigma^{\mathbf{x}} = \begin{pmatrix} \sigma_{x_1}^2 & \sigma_{x_{1,2}} & \cdots & \sigma_{x_{1,p}} \\ \sigma_{x_{2,1}} & \sigma_{x_2}^2 & \cdots & \sigma_{x_{2,p}} \\ \vdots & \vdots & \ddots & \vdots \\ \sigma_{x_{p,1}} & \sigma_{x_{p,2}} & \cdots & \sigma_{x_p}^2 \end{pmatrix}.$$
(16)

A

$p(x)$

1.96σ

μ_x

x

95% Confidence Interval

B

$\mathrm{Im}(x)$

Elliptical Confidence Area

μ_X

95% Confidence Interval

$|X|$

$\angle X$

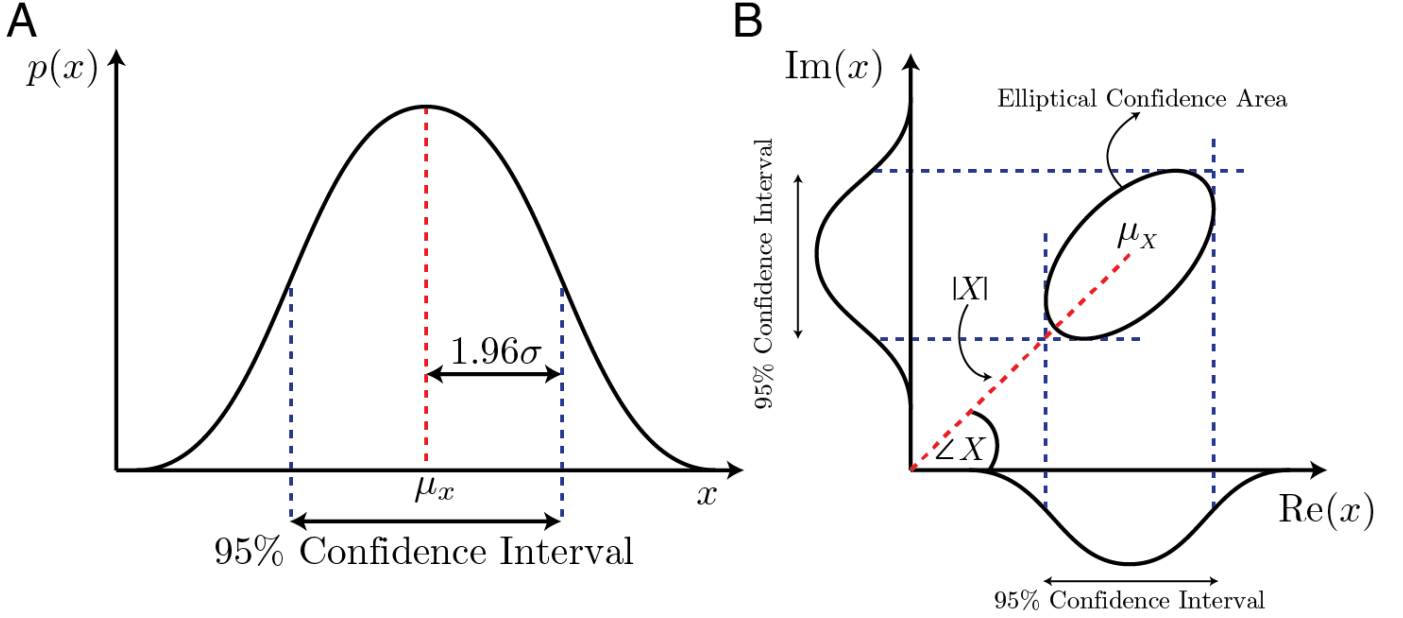$\mathrm{Re}(x)$

95% Confidence Interval

Fig. 1. The uncertainty in a complex variable can be represented by a bivariate normal distribution creating an elliptical uncertainty area in the real imaginary space. A) The probability distribution of a real valued univariate variable with its 95% confidence intervals. B) The elliptical confidence area of a complex variable represented by a bivariate normal distribution.

The variance of the output variable, y, is then given by [11]

$$\sigma_y^2 = \sum_i^p \sum_j^p c_i \Sigma_{ij}^{\mathbf{x}} c_j \tag{17}$$

In the general case f is allowed to take the form of some non-linear combination of $x_1, x_2, \ldots, x_p$ and a linearisation of f has to be performed (except in some special cases where the variance can be calculated exactly, see for example [25]). The classical propagation law is found by approximating f by a first order Taylor expansion

$$y \approx f_0 + \sum_{i=1}^p \frac{\partial f}{\partial x_i} x_i \tag{18}$$

which is valid only when the uncertainties associated with the input variables are small enough so that they satisfy the local linear approximation.

The variance of the non-linear function $f(x_1, x_2, \ldots, x_p)$ can be found from Equation (17) with

$$c_i = \frac{\partial f}{\partial x_i} \tag{19}$$

producing the classical law of uncertainty propagation

$$\sigma_y^2 = \sum_{i=1}^n \sum_{i=1}^n \frac{\partial f}{\partial x_i} \Sigma_{i,j}^{\mathbf{x}} \frac{\partial f}{\partial x_j}. \tag{20}$$

This method is used extensively for calculating errors in scientific measurements as recommended in *the Guide to the Expression of Uncertainty in Measurement* [11].

F. Multivariate uncertainty propagation

As shall be seen in Section II-G, when the output variable is complex valued it is necessary to consider a multivariate

form of the propagation law. The multivariate method allows for the estimation of uncertainty for multiple output variables simultaneously as well as the correlations between them.

The function f considered in the previous section is modified so that it is now a vector function denoted $\mathbf{f}$ of length q with a real valued vector output, $\mathbf{y}$, such that

$$\mathbf{y} = \mathbf{f}(\mathbf{x}) = \langle f_1(\mathbf{x}), f_2(\mathbf{x}), \ldots, f_q(\mathbf{x}) \rangle \tag{21}$$

The multivariate uncertainty propagation equation is then given by [13], [15], [26]

$$\Sigma^{\mathbf{y}} = \mathbf{J} \Sigma^x \mathbf{J}^T \tag{22}$$

where $\Sigma^{\mathbf{y}}$ is the covariance matrix for the output vector $\mathbf{y}$ and $\mathbf{J}$ is the Jacobian matrix given by

$$\mathbf{J} = \begin{bmatrix} \frac{\partial f_1}{\partial x_1} & \frac{\partial f_1}{\partial x_2} & \cdots & \frac{\partial f_1}{\partial x_p} \\ \frac{\partial f_2}{\partial x_1} & \frac{\partial f_2}{\partial x_2} & \cdots & \frac{\partial f_2}{\partial x_p} \\ \vdots & \vdots & \ddots & \vdots \\ \frac{\partial f_q}{\partial x_1} & \frac{\partial f_q}{\partial x_2} & \cdots & \frac{\partial f_q}{\partial x_p} \end{bmatrix} \tag{23}$$

Note that for a scalar output, Equation (22) reduces to the classical case given by (20). It is worth noting the similarity to the propagation step in the extended Kalman filter (EKF), which makes the same assumption that higher order terms in the Taylor series are negligible, based on the approximation of local linearity.

G. Propagation of uncertainty in complex valued variables

In order to incorporate the uncertainty analysis of complex valued variables a bivariate form of the propagation law is considered. The propagation of uncertainty in complex valued variables is developed in [13], [15], [26]. In these works both

the input and output variables of the function are complex valued. Here the input variables will be the real valued parameters of a time-domain, input-output model and only the output variable will be complex valued. The discussion presented here is based on the referenced work but considering a complex valued output only.

The complex valued output to some vector function f can be represented as the vector $\mathbf{y} = [y_1, y_2]$, where y_1 and y_2 represent the real and imaginary components of the output, such that

$$\mathbf{y} = \langle f_1(\mathbf{x}), f_2(\mathbf{x}) \rangle \tag{24}$$

where the functions $f_1(\mathbf{x})$ and $f_2(\mathbf{x})$ map the input vector $\mathbf{x}$ into the real and imaginary part of the output respectively.

The variance propagation equation is hence given by (22) where $\mathbf{J}$ is a $[2 \times p]$ Jacobian matrix given by

$$\mathbf{J} = \begin{bmatrix} \frac{\partial f_1}{\partial x_1} & \frac{\partial f_1}{\partial x_2} & \cdots & \frac{\partial f_1}{\partial x_p} \\ \frac{\partial f_2}{\partial x_1} & \frac{\partial f_2}{\partial x_2} & \cdots & \frac{\partial f_2}{\partial x_p} \end{bmatrix} \tag{25}$$

The covariance matrix representing the uncertainty associated with the input variables remains unchanged (*i.e.* is given by equation (16)).

This method therefore allows uncertainty to be approximately propagated through a function of multiple input variables into a complex output. It is now in the correct form to approximate the uncertainty in the complex valued FRF as a function of uncertain model parameters. The approach is adopted in the following section.

III. FREQUENCY RESPONSE UNCERTAINTY PROPAGATION FOR GENERAL INPUT-OUTPUT MODELS

In this section, variance propagation from a time-domain nonlinear system into the (complex-valued) frequency-domain is derived for the GFRF, the NOFRF and n^{th}-order output spectra. In addition, an algorithm for the complete model-based analysis of nonlinear systems is presented, from system identification in the time-domain, to generation of the frequency response functions and the associated uncertainty propagation novel to this paper.

A. Uncertainty propagation into the GFRF, NOFRF and n^{th}-order output spectra

The GFRF is a complex valued function, typically visualised in the space of the magnitude and phase. It is therefore desirable to propagate the parameter uncertainty, characterised by $\Sigma_{\boldsymbol{\theta}}$, directly into the bi-variate magnitude-phase space rather than the real-imaginary space given by (13). Employing the multivariate propagation law, given by (22), the covariance in the magnitude and phase of the GFRF, $H_n(j\omega_1, \ldots, j\omega_n)$, is given by

$$\Sigma_{|H_n|, \angle H_n} = \mathbf{J}_H(\omega, \boldsymbol{\theta}) \Sigma_{\boldsymbol{\theta}} \mathbf{J}_H(\omega, \boldsymbol{\theta})^T, \tag{26}$$

where

$$\mathbf{J}_H(\omega, \boldsymbol{\theta}) = \begin{bmatrix} \frac{\partial |H_n|}{\partial \theta_1} & \frac{\partial |H_n|}{\partial \theta_2} & \cdots & \frac{\partial |H_n|}{\partial \theta_M} \\ \frac{\partial \angle H_n}{\partial \theta_1} & \frac{\partial \angle H_n}{\partial \theta_2} & \cdots & \frac{\partial \angle H_n}{\partial \theta_M} \end{bmatrix} \tag{27}$$

where the GFRF covariance matrix is a function of the model parameters $\boldsymbol{\theta}$ and the frequencies $\omega_1, \ldots, \omega_n$. In order to evaluate (27), expressions for the partial differentials of the magnitude and phase with respect to the model parameters must be derived, which is performed in the next section.

Multivariate uncertainty propagation for the NOFRFs, $G_n(j\omega)$, can be similarly described as

$$\Sigma_{|G_n|, \angle G_n} = \mathbf{J}_G(\omega, \boldsymbol{\theta}) \Sigma_{\boldsymbol{\theta}} \mathbf{J}_G(\omega, \boldsymbol{\theta})^T, \tag{28}$$

where

$$\mathbf{J}_G(\omega, \boldsymbol{\theta}) = \begin{bmatrix} \frac{\partial |G_n|}{\partial \theta_1} & \frac{\partial |G_n|}{\partial \theta_2} & \cdots & \frac{\partial |G_n|}{\partial \theta_M} \\ \frac{\partial \angle G_n}{\partial \theta_1} & \frac{\partial \angle G_n}{\partial \theta_2} & \cdots & \frac{\partial \angle G_n}{\partial \theta_M} \end{bmatrix}. \tag{29}$$

and also noting that for arbitrary m

$$\frac{\partial G_n}{\partial \theta_m} = \frac{\int_{-\infty}^{\infty} \cdots \int_{-\infty}^{\infty} \frac{\partial H_n(j\omega_1, \ldots, j\omega_n)}{\partial \theta_m} \prod_{i=1}^{n} U(j\omega_i) d\omega_1 \ldots d\omega_n}{\int_{-\infty}^{\infty} \cdots \int_{-\infty}^{\infty} \prod_{i=1}^{n} U(j\omega_i) d\omega_1 \ldots d\omega_n} \tag{30}$$

Multivariate uncertainty propagation for the nth-order output spectra, $Y_n(j\omega)$, can also be described as

$$\Sigma_{|Y_n|, \angle Y_n} = \mathbf{J}_Y(\omega, \boldsymbol{\theta}) \Sigma_{\boldsymbol{\theta}} \mathbf{J}_Y(\omega, \boldsymbol{\theta})^T, \tag{31}$$

where

$$\mathbf{J}_Y(\omega, \boldsymbol{\theta}) = \begin{bmatrix} \frac{\partial |Y_n|}{\partial \theta_1} & \frac{\partial |Y_n|}{\partial \theta_2} & \cdots & \frac{\partial |Y_n|}{\partial \theta_M} \\ \frac{\partial \angle Y_n}{\partial \theta_1} & \frac{\partial \angle Y_n}{\partial \theta_2} & \cdots & \frac{\partial \angle Y_n}{\partial \theta_M} \end{bmatrix} \tag{32}$$

and also noting that

$$\frac{\partial Y_n}{\partial \theta_m} = \frac{n^{-1/2}}{(2\pi)^{n-1}} \int_{\omega} \frac{\partial H_n(j\omega_1, \ldots, j\omega_n)}{\partial \theta_m} \prod_{i=1}^{n} U(j\omega_i) d\sigma_{n\omega}. \tag{33}$$

B. Partial derivatives of magnitude and phase with respect to model parameters

The multivariate uncertainty propagation expressions for GFRFs, NOFRFs and the nth-order output spectra all require the definition of the partial derivative of the magnitude and phase with respect to the mth model parameter. Therefore, to avoid repetition we consider solving this problem for a general complex valued function, F, assuming we require $\frac{\partial |F_n|}{\partial \theta_m}$ and $\frac{\partial \angle F_n}{\partial \theta_m}$, for $m = 1, \ldots, M$.

1) Partial derivative of the magnitude: firstly, noting that

$$\text{Re}(F) = \frac{1}{2}(F + \overline{F}), \quad \text{Im}(F) = \frac{1}{2j}(F - \overline{F}) \tag{34}$$

where $\overline{F}$ represents the complex conjugate of F, and the partial derivative can be found by

$$
\begin{aligned}
\frac{\partial |F|}{\partial \theta_m} &= \frac{\partial}{\partial \theta_m}(F\overline{F})^{\frac{1}{2}} \\
&= \frac{\partial}{\partial F}(F\overline{F})^{\frac{1}{2}}\frac{\partial F}{\partial \theta_m} + \frac{\partial}{\partial \overline{F}}(F\overline{F})^{\frac{1}{2}}\frac{\partial \overline{F}}{\partial \theta_m} \\
&= \frac{1}{2}\overline{F}(F\overline{F})^{-\frac{1}{2}}\frac{\partial F}{\partial \theta_m} + \frac{1}{2}F(F\overline{F})^{-\frac{1}{2}}\frac{\partial \overline{F}}{\partial \theta_m} \\
&= \frac{1}{2|F|}\left(\overline{F}\frac{\partial F}{\partial \theta_m} + F\frac{\partial \overline{F}}{\partial \theta_m}\right) \\
&= \frac{1}{|F|}\operatorname{Re}\left(\overline{F}\frac{\partial F}{\partial \theta_m}\right).
\end{aligned}
\tag{35}
$$

2) Partial derivative of the phase: Taking the derivative of the angle of F

$$
\frac{\partial \angle F}{\partial \theta_m} = \frac{\partial}{\partial X}\arctan(X)\frac{\partial X}{\partial \theta_m},
\tag{36}
$$

where $X = \frac{\operatorname{Im}(F)}{\operatorname{Re}(F)}$. The derivative of X is given by

$$
\begin{aligned}
\frac{\partial X}{\partial \theta_m} &= \frac{\partial}{\partial \operatorname{Im}(F)}\left(\frac{\operatorname{Im}(F)}{\operatorname{Re}(F)}\right)\frac{\partial \operatorname{Im}(F)}{\partial \theta_m} \\
&\quad + \frac{\partial}{\partial \operatorname{Re}(F)}\left(\frac{\operatorname{Im}(F)}{\operatorname{Re}(F)}\right)\frac{\partial \operatorname{Re}(F)}{\partial \theta_m} \\
&= \frac{1}{\operatorname{Re}(F)}\frac{\partial \operatorname{Im}(F)}{\partial \theta_m} - \frac{\operatorname{Im}(F)}{\operatorname{Re}(F)^2}\frac{\partial \operatorname{Re}(F)}{\partial \theta_m}.
\end{aligned}
\tag{37}
$$

Employing equation (34) in Equation (37) leads to,

$$
\begin{aligned}
\frac{\partial X}{\partial \theta_m} &= \frac{1}{j}\left(\frac{\partial F}{\partial \theta_m} - \frac{\partial \overline{F}}{\partial \theta_m}\right)\frac{F + \overline{F}}{(F + \overline{F})^2} \\
&\quad - \frac{1}{j}\left(\frac{\partial F}{\partial \theta_m} + \frac{\partial \overline{F}}{\partial \theta_m}\right)\frac{F - \overline{F}}{(F + \overline{F})^2}
\end{aligned}
\tag{38}
$$

where the term on the left hand side has been multiplied by a factor of $F + \overline{F}$ in the numerator and denominator. Collecting terms

$$
\begin{aligned}
\frac{\partial X}{\partial \theta_m} &= \frac{2}{j(F + \overline{F})^2}\left(\overline{F}\frac{\partial F}{\partial \theta_m} - F\frac{\partial \overline{F}}{\partial \theta_m}\right) \\
&= \frac{4}{(F + \overline{F})^2}\operatorname{Im}\left(\overline{F}\frac{\partial F}{\partial \theta_m}\right) \\
&= \frac{1}{\operatorname{Re}(F)^2}\operatorname{Im}\left(\overline{F}\frac{\partial F}{\partial \theta_m}\right).
\end{aligned}
\tag{39}
$$

The derivative of $\arctan(X)$ is given by the identity

$$
\frac{\partial}{\partial X}\arctan(X) = \frac{1}{1 + X^2} = \frac{\operatorname{Re}(F)^2}{|F|^2}.
\tag{40}
$$

The general solution is then found by substituting equations (39) and (40) into Equation (36) such that,

$$
\frac{\partial \angle F}{\partial \theta_m} = \frac{1}{|F|^2}\operatorname{Im}\left(\overline{F}\frac{\partial F}{\partial \theta_m}\right).
\tag{41}
$$

C. Algorithm for frequency-domain uncertainty analysis of nonlinear systems

The frequency-domain uncertainty analysis for a nonlinear system can be performed using the following algorithm, which describes the full procedure, from standard steps of nonlinear system identification through to the novel frequency-domain uncertainty analysis derived in this paper.

The first step is to identify a time-domain nonlinear model of the system, if one is not already available,

1) (Optional) Time-domain identification of a nonlinear model of the system. The identified model must include an estimate of both the parameter means θ_μ and the parameter covariance Σ_θ.

Any suitable method can be used, e.g. for input design see [27], for identification algorithms see [20], [28]–[30] and for correlation-based validation methods see [31], [32].

The initial frequency-domain analysis can be performed using the identified model along with the following steps,

2) Calculate GFRFs, H_n, for $n = 1, \ldots, N$ using (7), where the procedure makes use of the time-domain model obtained in step 1, e.g as described in [3] or using an efficient algorithm as described in [22].
3) Calculate the nth-order input spectra using (10) for $n = 1, \ldots, N$.
4) Calculate the nth-order NOFRFs, for $n = 1, \ldots, N$, analytically using (9) or the data-driven algorithm in [4].
5) Filter the nth-order input spectra with the nth-order NOFRF to obtain the nth-order output spectra as described in (8).

Finally, the frequency-domain uncertainty analysis novel to this paper can be implemented by the following steps,

6) Calculate the partial derivatives of the GFRF with respect to the model parameters $\frac{\partial H_n}{\partial \theta_m}$ using the definition of H_n obtained in step 2.
7) Define $F = [F_1, \ldots, F_N]$, where F_n is the nth-order frequency domain description of interest, H_n, G_n, or Y_n.
8) Calculate the partial derivatives in gain, $\frac{\partial |F_n|}{\partial \theta_m}$, and phase, $\frac{\partial \angle F_n}{\partial \theta_m}$, using (35) and (41) respectively.
9) Define $\mathbf{J}_F(\omega, \boldsymbol{\theta})$ using (27), (29) or (32) respectively.
10) Calculate the uncertainty in gain and phase $\Sigma_{|F_n|, \angle F_n}$, for $n = 1, \ldots, N_m$ using (26), (28) or (31) respectively.

IV. Numerical examples

A. Nonlinear model uncertainty propagation for a simulated system

We demonstrate the procedure for propagating uncertainty into the frequency response for nonlinear systems using the following NARX model,

$$
\begin{aligned}
y_k &= \theta_1 y_{k-1} + \theta_2 y_{k-2} + \theta_3 u_{k-1} \\
&\quad + \theta_4 u_{k-2} + \theta_5 u_{k-1}^2 + \theta_6 y_{k-1}^2 + e_k
\end{aligned}
\tag{42}
$$

The first order GFRF is given by

$$
H_1(\omega, \boldsymbol{\theta}) = \frac{\theta_3 e^{-j\omega} + \theta_4 e^{-2j\omega}}{1 - \theta_1 e^{-j\omega} - \theta_2 e^{-2j\omega}}.
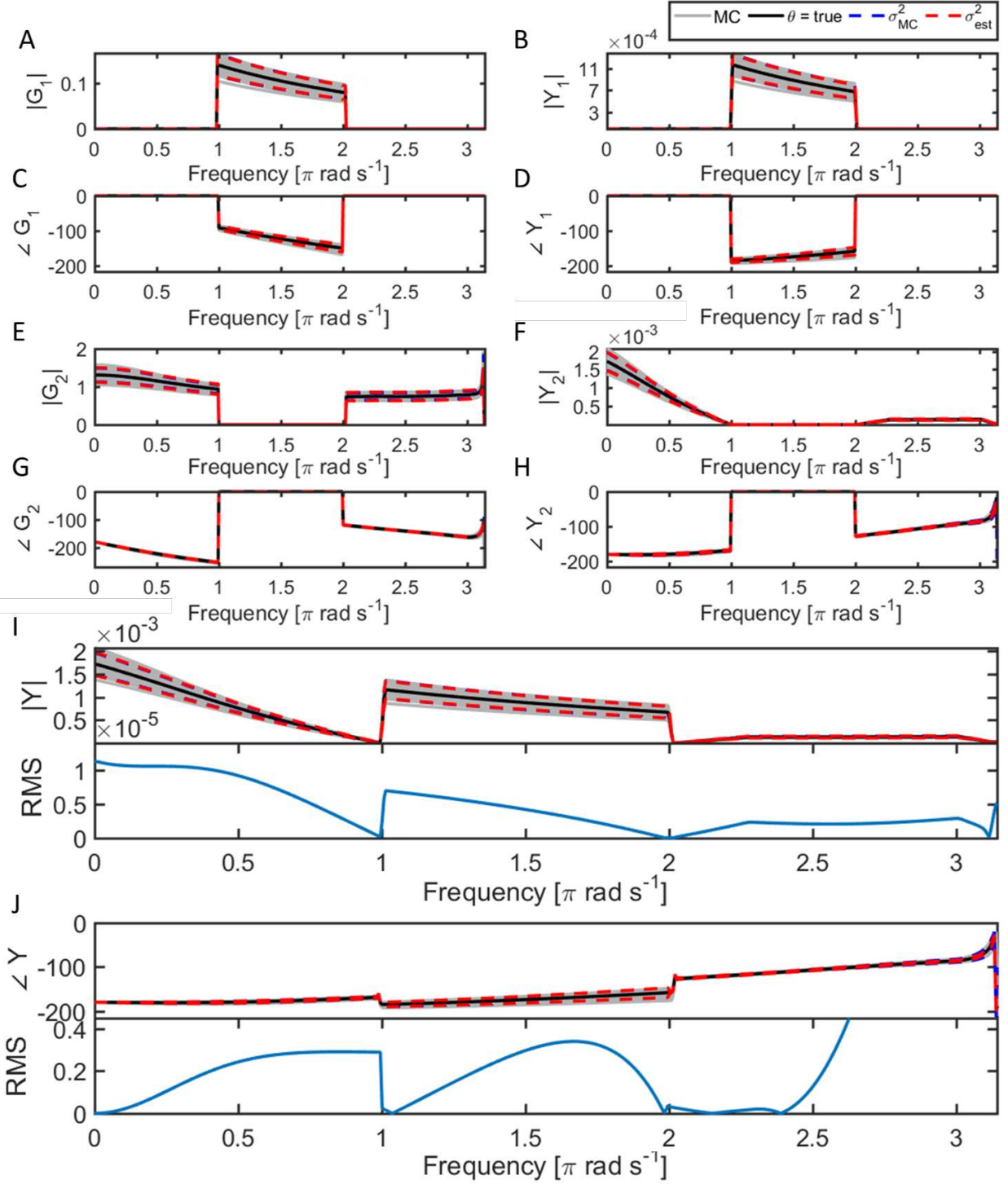\tag{43}
$$

Fig. 2. Comparison of frequency-domain uncertainty estimates generated by Monte Carlo sampling and uncertainty propagation for a simulated nonlinear system. True parameter values (Black), Monte Carlo samples (Grey), sampled variance (Blue dashed - note that the Red dashed line overlays the Blue dashed line in most instances) and propagated variance (Red dashed). A) Magnitude of G_1, B) Magnitude of Y_1, C) Phase of G_1, D) Phase of Y_1, E) Magnitude of G_2, F) Magnitude of Y_2, G) Phase of G_2, H) Phase of Y_2, I) Top: Magnitude of Y. Bottom: RMS error between estimated variance and propogated variance , and J) Top: Phase of Y. Bottom: RMS error between estimated variance and propogated variance.

The second order GFRF is given by

$$H_2(\omega_1, \omega_2) = \frac{\theta_5 e^{-j\pi(\omega_1+\omega_2)} + \theta_6 H_1(\omega_1) H_1(\omega_2) e^{-j\pi(\omega_1+\omega_2)}}{1 - \theta_1 e^{-j(\omega_1+\omega_2)} - \theta_2 e^{-2j(\omega_1+\omega_2)}}$$

(44)

Note that in general $H_1(\omega)$ cannot be a function of the parameters associated with higher order terms, in this case θ_5 and θ_6. However, higher order GFRFs may depend on lower order terms. Similarly, the partial derivatives of the nth-order GFRF may require the evaluation of lower order

partial derivatives. For example, differentiating $H_2(\omega_1, \omega_2)$ with respect to θ_1 gives

$$\frac{\partial H_2(\omega_1, \omega_2)}{\partial \theta_1} =$$

$$\frac{\theta_6 e^{-j\pi(\omega_1 + \omega_2)} \left(\frac{\partial H_1(\omega_1)}{\partial \theta_1} H_1(\omega_2) + \frac{\partial H_1(\omega_2)}{\partial \theta_1} H_1(\omega_1) \right)}{1 - \theta_1 e^{-j(\omega_1 + \omega_2)} - \theta_2 e^{-2j(\omega_1 + \omega_2)}} +$$

$$\frac{e^{-j\pi(\omega_1 + \omega_2)} \left(\theta_5 e^{-j\pi(\omega_1 + \omega_2)} + \theta_6 H_1(\omega_1) H_1(\omega_2) e^{-j\pi(\omega_1 + \omega_2)} \right)}{\left(1 - \theta_1 e^{-j(\omega_1 + \omega_2)} - \theta_2 e^{-2i(\omega_1 + \omega_2)} \right)^2}$$

(45)

which is dependent on $\frac{\partial H_1(\omega)}{\partial \theta_1}$. Although the differentiation is simple to perform it indicates that, in general, it is necessary to evaluate the differentials of all lower order FRFs.

To demonstrate the frequency-domain analysis procedure, the full algorithm given in section III.C was implemented here, beginning with identification of the model from simulated data. The system described by the nonlinear model in (42) was simulated for $N = 1000$ samples in response to an input excitation signal u_k drawn from a uniform distribution in the range $[-0.5, 0.5]$. The parameters were defined as $\boldsymbol{\theta} = (0.2, 0.1, 0.1, 0.05, 0.2, 0.5)^T$ and e_k was defined as an *i.i.d* white noise sequence drawn from the normal distribution $e_k \sim \mathcal{N}(0, \sigma_e^2)$ where $\sigma_e^2 = 0.0005$.

Model parameters were estimated using an algorithm based on variational Bayesian inference, which intrinsically generates parameter uncertainty [20]. The resulting posterior distribution for the parameters was normally distributed with mean and covariance given by

$$\mu_{\boldsymbol{\theta}} = \begin{bmatrix} 0.189 & 0.108 & 0.099 & 0.049 & 0.198 & 0.627 \end{bmatrix}^T$$

$$\Sigma_{\boldsymbol{\theta}} = 10^{-1} \times$$

$$\begin{bmatrix} 0.025 & -0.008 & 0.000 & -0.002 & -0.000 & -0.122 \\ -0.008 & 0.010 & -0.000 & 0.001 & -0.000 & 0.001 \\ 0.000 & -0.000 & 0.002 & -0.000 & -0.000 & 0.000 \\ -0.002 & 0.001 & -0.000 & 0.000 & 0.000 & 0.000 \\ -0.000 & -0.000 & -0.000 & 0.000 & 0.001 & -0.010 \\ -0.122 & 0.001 & 0.000 & 0.000 & -0.010 & 1.586 \end{bmatrix}$$

In this example, only the NOFRF and the output spectra were analysed. This is because the first order GFRF contains similar information to the first order NOFRF and so is redundant, whilst the second order GFRF is 2-dimensional and is therefore difficult to analyse, whilst higher order GFRFs cannot be visualised at all. In the general case, it would appear simpler to take this approach and focus on the NOFRF, which also has the advantage of being input-specific. Also, note that we only analyse the magnitude (or gain) of the nonlinear system here, which is most interesting for checking phenomena such as resonances, super/sub-harmomics and energy transfer across frequencies.

The covariance in the NARX model parameters was propagated into the nth-order NOFRF and the nth-order output spectra using (28)-(29) and (31)-(32) respectively. The input signal used to evaluate the NOFRF was uniform across frequencies in the band $[1, 2]$ rad s^{-1} and zero elsewhere, see [4] for the generation of such a signal. Monte Carlo sampling was used as a comparison to benchmark and validate the approach for uncertainty propagation, using $N_{MC} = 100$ samples (the number of samples was relatively small because the computational cost of repeatedly performing the frequency-domain mapping is prohibitively expensive). The evaluation of the NOFRFs for the true parameter vector took 0.89 seconds with a further 0.068 seconds to propagate the uncertainty with timings averaged over 100 runs. The evaluation of NOFRFs for $N_{MC} = 100$ samples took 88.7 seconds. Computations were performed on a laptop computer with an intel(r) core(tm) i7 CPU @ 2.GHz processor and 8GB RAM.

The propagated variance in the gain and phase of both the NOFRF and the nth-order output spectra showed good agreement to the sampled variance in all cases, see Figure 2A-H. The output spectrum was approximated as $Y \approx Y_1 + Y_2$, assuming higher orders have a negligible contribution to the output. The variance in the gain and phase of the output spectrum was calculated as $\sigma_Y^2 = \sigma_{Y_1}^2 + \sigma_{Y_2}^2$ and similarly shows good agreement to the sampled variance, see Figure 2I-J. The error between the propogated variance and the MC sampled variance on both the gain and phase is shown in Figure (2) I and J respectively, where the error is expressed as the root mean square error. Errors are only shown for Y, given that the first and second order frequency spectra are located at exclusive frequency bands, the errors of the individual orders can be inferred. Normalised errors are identical for G_i and Y_i, this is explained by noting that the source of error in both Equations (30) and (33) originate from H_i. RMS errors are small in both gain and phase for low frequencies, large errors are observed in the phase at high frequencies (> 2.5 rad s^{-1}).

B. Nonlinear model uncertainty propagation for a real-world experimental system

In this section the uncertainty propagation method is applied to characterising the frequency domain uncertainty of a class of soft-smart actuator known as a dielectric elastomer actuator (DEA), a type of electroactive polymer used in robotics that is known to display nonlinear behaviour [33]. Due to the wide fabrication tolerances of DEA uncertainty characterisation is particularly pertinent. The experimental set up and data collection procedure has been described before [34], therefore only a brief description is given here to put the case study into context.

The experimental set-up consisted of a custom fabricated DEA formed by stretching a transparent, biaxially pre-strained circular acrylic elastomer (3M VHB 4905) over a perspex frame, with inner and outer diameters of 80 mm and 120 mm respectively, see Figure 3A. Electrodes made from conductive carbon grease (MG chemicals) were attached to both sides of the elastomer. A weighted ball (3g) was placed centrally on the upper side of the elastomer. Applying a voltage (system input) across the electrodes causes bi-axial (in-plane) expansion, inducing vertical (out-of-plane) displacement (system output). The displacement was measured with a laser displacement sensor. The excitation voltage was band limited white noise, designed for the purpose of system identification, see Figure 3B.
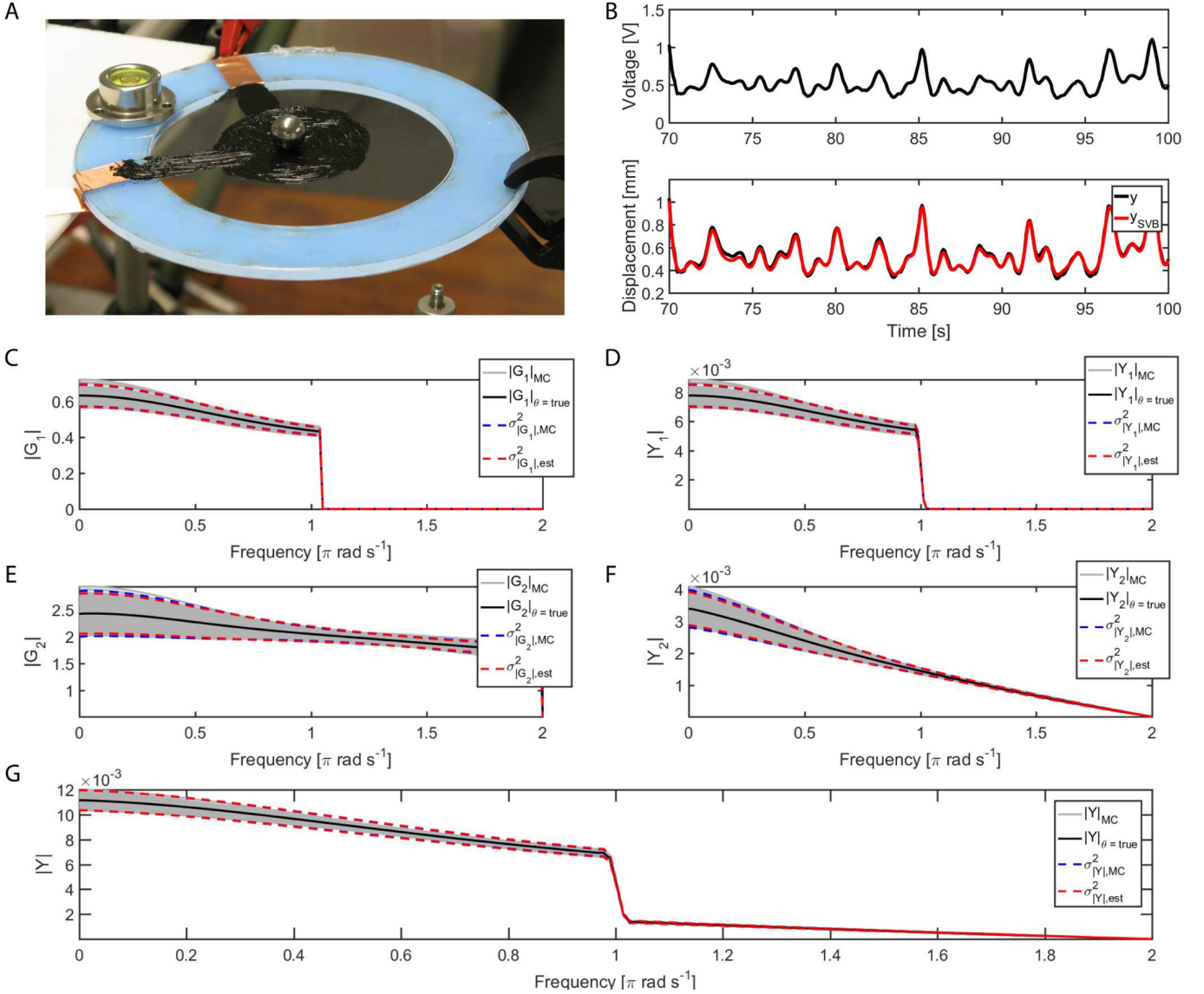
Fig. 3. Comparison of frequency-domain uncertainty estimates generated by Monte Carlo sampling and uncertainty propagation for identified nonlinear models of two dielectric elastomer actuators (DEAs). A) Picture of the DEA experimental set-up. B) Top: DEA system input (Voltage). Bottom: measured DEA system output (Displacement) DEA system (Black) with the model predicted output of the model identified with the SVB-NARX algorithm (Red). C-G) True parameter values (Black) with the Monte Carlo samples (Grey), sampled variance (Blue dashed - note that the Red dashed line overlays the Blue dashed line in most instances) and propagated variance (Red dashed) for experiment 1. C) Magnitude of G_1, D) Magnitude of Y_1, E) Magnitude of G_2, F) Magnitude of Y_2 and G) Magnitude of Y.

The DEA nonlinear model was identified using the sparse variational Bayes-NARX (SVB-NARX) algorithm described in [20], which produced a model with accurate predictive capability, see Figure 3B. First and second order GFRFs, NOFRFs and output spectra were calculated for the DEA using the identified model, along with the variance using uncertainty propagation proposed here. Monte Carlo sampling was also used to generate numerical estimates of the variance for a comparison to uncertainty propagation. The propagated variance in the NOFRFs and output spectra closely matched the variance in the gain of the sampled output spectra, see Figure 3C-G.

The close agreement between the uncertainty propagation method and Monte Carlo sampling demonstrates the effec-

tiveness of uncertainty propagation, which avoids the computational cost of sampling. Uncertainty propagation, therefore, provides a valuable addition to methods used in the analysis of nonlinear systems.

V. SUMMARY

In this paper a novel approach has been developed for the frequency-domain uncertainty analysis of nonlinear systems. The method uses multivariate uncertainty propagation to estimate the frequency-domain uncertainty characteristics from the distribution of the time-domain model parameters. The analysis procedure was demonstrated using both simulated and real-world examples. In both cases it was shown that the propagation procedure closely resembles the result acquired by

Monte Carlo sampling from the model parameter distribution in order to build up a posterior distribution in the frequency-domain. A key advantage of the uncertainty propagation method is that it avoids the repeated sampling involved in Monte Carlo simulations and the associated computational cost. Uncertainty propagation is therefore a useful and important addition to the suite of tools used in the analysis of nonlinear systems.

APPENDIX

A. Direct evaluation of NOFRFs

This section describes the direct evaluation of NOFRFs from time-domain model simulations (as opposed to their indirect evaluation via GFRFs) using the method defined in [4].

Firstly, note that the output spectra of a nonlinear system as defined in (8) can be re-written as a function of the NOFRFs in the following form,

$$Y(j\omega) = \sum_{n=1}^{N} Y_n(j\omega) = \sum_{n=1}^{N} G_n(j\omega)U_n(j\omega)$$
$$= \sum_{n=1}^{N} G_n(j\omega)\alpha^n U_n^*(j\omega) \tag{46}$$

where $G_n(j\omega)$ is the nth-order NOFRF, and the input frequency spectra of a specific time-domain input $u(t) = \alpha u^*(t)$ is defined as

$$U_n(j\omega) = \frac{n^{-1/2}}{2\pi^{n-1}} \int_{-\infty}^{\infty} \cdots \int_{-\infty}^{\infty} \prod_{i=1}^{n} U(j\omega_i) d\omega_1 \ldots d\omega_n$$
$$= \alpha^n \frac{n^{-1/2}}{2\pi^{n-1}} \int_{-\infty}^{\infty} \cdots \int_{-\infty}^{\infty} \prod_{i=1}^{n} U^*(j\omega_i) d\omega_1 \ldots d\omega_n$$
$$= \alpha^n U_n^*(j\omega) \tag{47}$$

where $U^*(j\omega)$ is the Fourier transform of $u^*(t)$ and

$$U_n^*(j\omega) = \frac{n^{-1/2}}{2\pi^{n-1}} \int_{-\infty}^{\infty} \cdots \int_{-\infty}^{\infty} \prod_{i=1}^{n} U^*(j\omega_i) d\omega_1 \ldots d\omega_n \tag{48}$$

The key idea for estimating the NOFRFs is to define a representation of (46) based on numerical samples of frequency-domain transformations of time-domain input-output data, generated from K time-domain model simulations, where $K \geq N$. The K model simulations each use a distinct input signal, $\alpha_i u^*(t)$, for $i = 1, \ldots, K$, where a single waveform, $u^*(t)$, is scaled by increasing amplitudes defined by α_i, where $\alpha_K > \alpha_{K-1} > \ldots > \alpha_1 > 0$, leading to

$$\mathbf{Y} = \mathbf{U}\mathbf{G} \tag{49}$$

where

$$\mathbf{Y} = [Y_1^*(j\omega), \ldots, Y_K^*(j\omega)]^T \tag{50}$$

$$\mathbf{U} = \begin{bmatrix} \alpha_1 U_1^*(j\omega) & \cdots & \alpha_1^N U_N^*(j\omega) \\ \vdots & & \vdots \\ \alpha_K U_1^*(j\omega) & \cdots & \alpha_K^N U_N^*(j\omega) \end{bmatrix} \tag{51}$$

$$\mathbf{G} = [G_1(j\omega), \ldots, G_N(j\omega)]^T \tag{52}$$

where $Y_i^*(j\omega)$ for $i = 1, \ldots, K$ is the frequency-domain transformation of the corresponding time-domain output signal from the model simulation, $y_i^*(t)$ for $i = 1, \ldots, K$, which can be obtained in practice by taking the fast Fourier transform (FFT) of $y_i^*(t)$. Note also that the terms $U_i^*(j\omega)$, for $i = 1, \ldots, K$, can be obtained in practice by taking the FFT of $(u^*(t))^i$, for $i = 1, \ldots, K$.

Given $\mathbf{Y}$ and $\mathbf{U}$ it is straightforward to estimate the NOFRFs in closed form via

$$\hat{\mathbf{G}} = \left(\mathbf{U}^{\mathrm{H}}\mathbf{U}\right)^{-1} \mathbf{U}^{\mathrm{H}}\mathbf{Y} \tag{53}$$

where $\mathbf{U}^{\mathrm{H}}$ denotes the conjugate transpose of $\mathbf{U}$.

Once the NOFRFs have been estimated, the nth-order output spectra can also be reconstructed as

$$Y_n(j\omega) = \hat{G}_n(j\omega)U_n(j\omega) \text{ for } n = 1, \ldots, N \tag{54}$$

where $\hat{G}_n$ is an element of $\hat{\mathbf{G}}$ and $U_n(j\omega)$ is the FFT of $(u(t))^n$, for $n = 1, \ldots, N$.

REFERENCES

[1] L. Ljung, *System identification: theory for the user*, 2nd ed., ser. Prentice Hall information and system sciences series. Upper Saddle River, NJ: Prentice Hall PTR, 1999.

[2] S. A. Billings, *Nonlinear system identification: NARMAX methods in the time, frequency, and spatio-temporal domains.* Wiley, 2013.

[3] S. A. Billings and K. M. Tsang, "Spectral analysis for non-linear systems, Part I: Parametric non-linear spectral analysis," *Mechanical Systems and Signal Processing*, vol. 3, no. 4, pp. 319–339, 1989.

[4] Z. Q. Lang and S. A. Billings, "Energy transfer properties of non-linear systems in the frequency domain," *International Journal of Control*, vol. 78, no. 5, pp. 345–362, Mar. 2005.

[5] H. Zhang and S. Billings, "Analysing non-linear systems in the frequency domain–I. the transfer function," *Mechanical Systems and Signal Processing*, vol. 7, no. 6, pp. 531–550, 1993.

[6] Z. Peng, Z.-Q. Lang, and S. Billings, "Resonances and resonant frequencies for a class of nonlinear systems," *Journal of Sound and Vibration*, vol. 300, no. 3, pp. 993–1014, 2007.

[7] G. C. Goodwin, M. Gevers, and B. Ninness, "Quantifying the error in estimated transfer functions with application to model order selection," *IEEE Transactions on Automatic Control*, vol. 37, no. 7, pp. 913–928, 1992.

[8] B. Wahlberg and L. Ljung, "Hard frequency-domain model error bounds from least-squares like identification techniques," *IEEE Transactions on Automatic Control*, vol. 37, no. 7, pp. 900–912, 1992.

[9] X. Bombois, B. Anderson, and M. Gevers, "Frequency domain image of a set of linearly parametrized transfer functions," in *European Control Conference (ECC)*, 2001, pp. 1416–1421.

[10] K. Worden, "Confidence bounds for frequency response functions from time series models." *Mechanical Systems and Signal Processing*, vol. 12, no. 4, pp. 559–569, Jul. 1998.

[11] Bureau International des Poids et Mesures, *Guide to the Expression of Uncertainty in Measurement*. International Organization for Standardization, 1995.

[12] R. Pintelon and J. Schoukens, "Measurement of frequency response functions using periodic excitations, corrupted by correlated input/output errors," *IEEE Transactions on Instrumentation and Measurement*, vol. 50, no. 6, pp. 1753–1760, 2001.

[13] N. M. Ridler and M. J. Salter, "An approach to the treatment of uncertainty in complex S-parameter measurements," *Metrologia*, vol. 39, no. 3, p. 295, 2002.

[14] B. D. Hall, "Calculating measurement uncertainty for complex-valued quantities," *Measurement Science and Technology*, vol. 14, no. 3, p. 368, 2003.

[15] ——, "On the propagation of uncertainty in complex-valued quantities," *Metrologia*, vol. 41, no. 3, pp. 173–177, Jun. 2004.

[16] T. Schultz, M. Sheplak, and L. N. Cattafesta, "Application of multivariate uncertainty analysis to frequency response function estimates," *Journal of Sound and Vibration*, vol. 305, no. 1-2, pp. 116–133, Aug. 2007.

[17] Thomas E. Fricker, J. E. Oakley, N. D. Sims, and K. Worden, "Probabilistic uncertainty analysis of an FRF of a structure using a Gaussian process emulator," *Mechanical Systems and Signal Processing*, vol. 25, no. 8, pp. 2962–2975, 2011.

[18] O. Nelles, *Nonlinear System Identification*. Berlin: Springer, 2001.

[19] J. Sjöberg, Q. Zhang, L. Ljung, A. Benveniste, B. Delyon, P.-Y. Glorennec, H. Hjalmarsson, and A. Juditsky, "Nonlinear black-box modeling in system identification: a unified overview," *Automatica*, vol. 31, no. 12, pp. 1691–1724, 1995.

[20] W. R. Jacobs, T. Baldacchino, T. J. Dodd, and S. R. Anderson, "Sparse bayesian nonlinear system identification using variational inference," *IEEE Transactions on Automatic Control*, 2018.

[21] T. Baldacchino, S. R. Anderson, and V. Kadirkamanathan, "Structure detection and parameter estimation for NARX models in a unified EM framework," *Automatica*, vol. 48, no. 5, pp. 857–865, May 2012.

[22] J. P. Jones and K. Choudhary, "Efficient computation of higher order frequency response functions for nonlinear systems with, and without, a constant term," *International Journal of Control*, vol. 85, no. 5, pp. 578–593, May 2012.

[23] A. Lyon, "Why are normal distributions normal?" *The British Journal for the Philosophy of Science*, vol. 65, no. 3, pp. 621–649, 2014.

[24] W. K. Härdle and L. Simar, *Applied Multivariate Statistical Analysis*. Berlin, Heidelberg: Springer Berlin Heidelberg, 2012.

[25] L. A. Goodman, "On the Exact Variance of Products," *Journal of the American Statistical Association*, vol. 55, no. 292, p. 708, Dec. 1960.

[26] R. Willink and B. D. Hall, "A classical method for uncertainty analysis with multidimensional data," *Metrologia*, vol. 39, no. 4, p. 361, 2002.

[27] I. Leontaritis and S. Billings, "Experimental design and identifiability for non-linear systems," *International Journal of Systems Science*, vol. 18, no. 1, pp. 189–202, 1987.

[28] S. Chen, S. A. Billings, and W. Luo, "Orthogonal least squares methods and their application to non-linear system identification," *International Journal of Control*, vol. 50, no. 5, pp. 1873–1896, Nov. 1989.

[29] L. Piroddi and W. Spinelli, "An identification algorithm for polynomial NARX models based on simulation error minimization," *International Journal of Control*, vol. 76, no. 17, pp. 1767–1781, Nov. 2003.

[30] T. Baldacchino, S. R. Anderson, and V. Kadirkamanathan, "Computational system identification for Bayesian NARMAX modelling," *Automatica*, vol. 49, no. 9, pp. 2641–2651, Sep. 2013.

[31] S. A. Billings and W. S. F. Voon, "Correlation based model validity tests for non-linear models," *International Journal of Control*, vol. 44, no. 1, pp. 235–244, Jul. 1986.

[32] S. Billings and Q. Zhu, "Nonlinear model validation using correlation tests," *International Journal of Control*, vol. 60, no. 6, pp. 1107–1120, 1994.

[33] Y. Bar-Cohen, Ed., *Electroactive polymer (EAP) actuators as artificial muscles: reality, potential, and challenges*, 2nd ed. Bellingham, Wash: SPIE Press, 2004.

[34] W. R. Jacobs, E. D. Wilson, T. Assaf, J. Rossiter, T. J. Dodd, J. Porrill, and S. R. Anderson, "Control-focused, nonlinear and time-varying modelling of dielectric elastomer actuators with frequency response analysis," *Smart Materials and Structures*, vol. 24, no. 5, p. 055002, May 2015.

William R. Jacobs received the M.Phys. degree in physics with mathematics from the University of Sheffield, Sheffield, UK, in 2010 and the Ph.D. degree in nonlinear system identification from the University of Sheffield in 2016.

He is currently working as a Research Associate in the Rolls Royce University Technology Centre, Department of Automatic Control and Systems Engineering at the University of Sheffield.

Tony Dodd received the B.Eng. degree in aerospace systems engineering from the University of Southampton, Southampton, UK, in 1994 and the Ph.D. degree in machine learning from the Department of Electronics and Computer Science, University of Southampton in 2000.

From 2002 to 2010, he was a Lecturer in the Department of Automatic Control and Systems Engineering at the University of Sheffield, Sheffield, UK, and from 2010 to 2015 was a Senior Lecturer at the University of Sheffield. He is currently a Professor of Autonomous Systems Engineering and Director of the MEng Engineering degree programme at the University of Sheffield.

Sean R. Anderson received the M.Eng. degree in control systems engineering from the Department of Automatic Control and Systems Engineering, University of Sheffield, Sheffield, UK, in 2001 and the Ph.D. degree in nonlinear system identification and predictive control from the University of Sheffield in 2005.

From 2005 to 2010, he was a Research Associate in the Neural Algorithms Research Group, University of Sheffield. From 2010 to 2012 he was a Research Associate in the Department of Automatic Control and Systems Engineering, University of Sheffield and has been a senior lecturer there since 2015.